Computer simulation study of the structure of the liquid-vapor interface of mercury at 20, 100, and 200 °C

Dmitriy S. Chekmarev, Meishan Zhao, and Stuart A. Rice
Department of Chemistry and The James Franck Institute, The University of Chicago, Chicago, Illinois 60637
(Received 20 July 1998)

We report the results of self-consistent quantum Monte Carlo simulations of the liquid-vapor interface of Hg. Our calculations are intended to answer two questions: (i) What is the quality of agreement between experimental data and calculations of the structure of the liquid-vapor interface of Hg based on the best available treatment of an inhomogeneous liquid metal? (ii) How well does a theory of the liquid-vapor interface of a metal that uses a simple model local pseudopotential reproduce the predictions obtained from a theory that uses an accurate nonlocal pseudopotential? As for the liquid-vapor interfaces of other metals, we find that the density distribution along the normal to the liquid-vapor interface of Hg (the longitudinal density distribution) is stratified, with a penetration depth into the bulk liquid of about three layers. The use of a nonlocal pseudopotential in the self-consistent Monte Carlo simulations leads to very good agreement between the calculated and observed longitudinal density distributions. We also show that the use of a model local pseudopotential leads to a qualitatively correct description of the longitudinal density in the liquid-vapor interface of Hg. When the model local pseudopotential is used, the locations of the strata in the longitudinal density distribution are correct but the peak heights are too large and the peak widths are too small. The largest part of the error arising from the use of the model local pseudopotential can be traced to the error in the predicted surface tension. The quality of the agreement between simulations based on the best nonlocal pseudopotential and those based on a simple model local pseudopotential is sufficient to make the latter a very useful tool for inferring the qualitative properties of a broad class of inhomogeneous liquid metals and alloys. We also report the results of calculations of the transverse (in-plane) structure of the liquid-vapor interface of Hg, for several slices of the interface. Except in the outermost layer, the transverse pair correlation function is found to be indistinguishable for the bulk liquid pair correlation function, in agreement with the available experimental data. Unlike the case of the liquid-vapor interface of alkali metals, our results imply there is a nontrivial difference between the transverse pair correlation function in the outermost layer of the liquid-vapor interface of Hg and that in the bulk liquid. The difference takes the form of an exaggerated shoulder on the first peak of the pair correlation function and is of the type which some investigators believe is associated with dimerization. However, we can find no direct evidence for dimer formation in images from our simulations of the positions of the ion cores in the outermost layer of the liquid-vapor interface of Hg.
[S1063-651X(99)04401-3]

PACS number(s): 68.10.−m, 61.20.−p, 68.35.Ct

I. INTRODUCTION

The initial development of the theory of metals was primarily concerned with understanding the influence of the field of a three dimensional periodic lattice of ion cores on the energy spectrum of a free electron gas. One important consequence of those studies is the association of the metallic character of a crystalline material with the existence of broad, delocalized, partially filled electronic energy bands, while the thermal displacements of the ion cores from the lattice positions generate small perturbations that limit the electron mobility. This version of the theory of metals is not immediately applicable to liquids because of the absence of an underlying periodic lattice which can be used to characterize the static distribution of ion cores in the liquid. It was the development of the nearly free electron (NFE) theory of homogeneous liquid metals in the 1960s, by Ziman and coworkers, that first provided a satisfactory representation of the relationship between electronic structure, electron transport properties, and the distribution of ion cores in a liquid [1]. Numerous accounts of the applications of this theory to the calculation of diverse thermodynamic and transport properties of bulk liquid metals can now be found in the literature [2]. In contrast, our understanding of the structure and electronic properties of inhomogeneous liquid metal systems, for example, the liquid-vapor and liquid-crystal interfaces of metals, has progressed very slowly. That slow progress is, in part, due to the necessity to construct a theoretical description of a two-component, spatially nonuniform, partially disordered distribution of ion cores and valence electrons with allowance for the occurrence of a metal-to-nonmetal transition and, in part, due to the paucity of experimental data with which to test the predictions of, and with which to challenge the interpretations of, the proposed theoretical analyses. However, there is now available a combination of theoretical developments [3], of improvements in computer simulation methodology [4,5], and of advances in x-ray reflection [6–12] and grazing incidence x-ray diffraction methodologies [13–16] that provides the tools needed for the comprehensive investigation of the structural properties of inhomogeneous metals.

The liquid-vapor interface is a self-supporting region separating coexisting gaseous and liquid phases which have very different densities, hence it is a natural vehicle for the

study of the properties of inhomogeneous fluids. It is now firmly established that the structure of the liquid-vapor interface of a simple fluid depends on features of the intermolecular potential which are different in dielectric and metals. In a dielectric liquid, whose potential energy is adequately represented by a sum of density independent pair interactions, the longitudinal density profile in the liquid-vapor interface (i.e., along the normal to the interface) monotonically decreases as one passes from the bulk liquid side to the vapor side of the interface; near the triple point of the liquid the width of that profile is about two to three molecular diameters [17–19]. In contrast, in a liquid metal the interaction between a pair of ion cores has a strong dependence on the electron density, so the pair interactions in the liquid-vapor interface depend on position along the normal to the interface. In this case the longitudinal density distribution in the liquid-vapor interface has pronounced oscillations; near the freezing point of the metal these oscillations penetrate three to four atomic diameters into the bulk liquid [6–11,20–29,19]. The stratification of the liquid-vapor interface of a metal can be interpreted as a signature of the strong confining force exerted on the ion cores in the interface, and the confining force can be traced to the density dependence of the volume term in the potential energy functional of the electron-ion core system.

The most useful current theoretical description of the structure of a liquid metal-vapor interface is derived from self-consistent quantum Monte Carlo simulations. The analytical basis for the simulations, as developed by D'Evelyn and Rice [20,21] and later refined by Harris, Gryko, and Rice [22,23], is the density functional pseudopotential representation of the properties of an inhomogeneous metal. The calculation of the nonlocal pseudopotential requires, as input, the electron density distribution in the interface; this distribution is obtained from the solution to the relevant Kohn-Sham equation [30]. The nonlocal pseudopotential of the system is then used in a Monte Carlo simulation of the system properties. Since the local electron density changes when the ion cores are moved, the pseudopotential must be recalculated after each Monte Carlo move. This procedure, when carried to convergence, generates self-consistent electron and in core distributions for the metal. To date, the procedure described has been used to study the liquid-vapor interfaces of Na, Cs, Hg, Mg, Ga, Al, In, Tl, and the dilute alloys BiGa and InGa [24–26,28,29]. In general, there is very good agreement between the predicted [25–28] and experimentally inferred [6,9,11,12,16] longitudinal density distributions in the liquid-vapor interfaces of Ga, BiGa, and InGa. The character of this agreement suggests that the extent theory can be used as a reliable predictor of the properties of other inhomogeneous liquid metal systems. However, the calculations of the properties of the systems just cited utilize a sophisticated nonlocal representation of the atomic interactions, and require very extensive and lengthy computations. Moreover, the formalism does not provide a simple conceptual picture of the elements of the interaction which are most important for the determination of the structure of the liquid-vapor interface of a metal, hence there is no simple way of inferring the qualitative properties of a broad class of inhomogeneous metals and alloys from knowledge of their nonlocal pseudopotentials.

This paper is concerned with two issues: (i) What is the quality of the agreement between the predicted and observed density distribution along the normal to the liquid-vapor interface of Hg? (ii) How well does a theory of the liquid-vapor interface structure which uses a simple local pseudopotential reproduce the predictions obtained from a theory which uses an accurate nonlocal pseudopotential?

We are aware of only one previous theoretical study of the structure of the liquid-vapor interface of Hg, by D'Evelyn and Rice [20]. They reported the results of self-consistent Monte Carlo simulations of the liquid-vapor interface of a small spherical cluster of 256 atoms. In the execution of the simulations they imposed the condition of local electroneutrality and included, through a semiempirical ansatz, the occurrence of a metal-to-nonmetal transition in the liquid-vapor interface. We note that imposition of the constraint of local electroneutrality requires that the ion core and electron charge distributions be identical, which is an approximation that compromises the accuracy of the predicted longitudinal density distribution. Indeed, the D'Evelyn-Rice results can only yield a qualitative description of the structure of the liquid-vapor interface of Hg. Improvement of the quality of the theoretical prediction of the structure of the liquid-vapor interface of Hg is one of the objectives of the studies reported in this paper.

Chekmarev, Zhao, and Rice [19] have reported the results of self-consistent Monte Carlo simulation studies of the structure of the liquid metal-vapor interface based on use of a modified semiempirical empty-core model potential. The predicted structures of the liquid-vapor interfaces of Na and Cs were found to agree very well with the structures obtained from previous simulation studies [22] which were based on use of a complicated nonlocal pseudopotential. In this paper we pursue further the idea of constructing a simplified, qualitatively sound, description of the liquid-vapor interface of a metal by extending the local model potential formalism [19] to the case of a polyvalent metal, namely, Hg. Our goals are to test the accuracy of the local model potential formalism against the predictions made using a nonlocal pseudopotential representation, and to test the accuracy of both against the experimentally inferred longitudinal density distribution in the liquid-vapor interface of Hg [7].

Bulk Hg is one of a class of liquid metals in which there are complex, possibly noncentral, atomic interactions; the signature of membership in this class is commonly taken to be the asymmetry of the first peak of the static structure function $S(q)$ [31–33]. The asymmetry typically takes the form of a broad ''shoulder'' on the large q side of the first peak of $S(q)$ [33]. Liquid metals in this class can be deeply supercooled, and they exhibit polymorphism in their solid phases [31,33]. It is argued by some investigators [31,34] that the local ordering in liquid Hg is reminiscent of the rhombohedral ordering found in solid αHg (though this interpretation has not been confirmed in other studies [35]). Accepting that the atomic interactions in liquid Hg are complex, what is the structural response to the variation of the valence electron and ion densities across the interface? Is it reasonable to expect unusual ordering of the ion cores in the inhomogeneous region separating the bulk liquid and the vapor, and will that ordering be sensitive to variation of the temperature? As for the liquid-vapor interfaces of other metals, we find that the longitudinal density distribution in the

liquid-vapor interface of Hg is stratified, with a penetration depth into the bulk liquid of about three layers. We find that the use of a nonlocal pseudopotential in the self-consistent Monte Carlo simulations leads to very good agreement between the calculated and observed longitudinal density distributions. We also show that the use of a model local pseudopotential leads to a qualitatively correct description of the longitudinal density distribution in the liquid-vapor interface of Hg. When the model local pseudopotential is used, the locations of the strata in the longitudinal density distribution are correct but the peak heights are too large and the peak widths are too small. The largest part of the error arising from the use of the model local pseudopotential can be traced to the error in the predicted surface tension. The quality of the agreement between simulations based on the best nonlocal pseudopotential and those based on a simple model local pseudopotential is sufficient to make the latter a very useful tool for inferring the qualitative properties of a broad class of inhomogeneous liquid metals and alloys.

We also report the results of calculations of the transverse (in-plane) structure of the liquid-vapor interface of Hg, for several slices of the interface. Except in the outermost layer of the liquid-vapor interface, the transverse pair correlation function is found to be indistinguishable from the bulk liquid pair correlation function, in agreement with the available experimental data. Unlike the case of the liquid-vapor interface of alkali metals, our results imply there is a nontrivial difference between the transverse pair correlation function in the outermost layer of the liquid-vapor interface of Hg and that in the bulk liquid. This difference takes the form of an exaggerated shoulder on the first peak of the pair correlation function and is of the type which some investigators believe is associated with dimerization. However, we can find no direct evidence for dimer formation in images from our simulations of the positions of the ion cores in the outermost layer of the liquid-vapor interface of Hg.

II. THEORETICAL BACKGROUND

We have carried out self-consistent quantum Monte Carlo simulations of the structure of the liquid-vapor interface of Hg using both an accurate nonlocal pseudopotential [the energy independent model potential (EIMP) [36]] and a simple model potential. The general methodology associated with both forms of the pseudopotential is the same; it has been described in detail in our previous papers [21,25,19], and will not be repeated here. It is sufficient to note that, following D'Evelyn and Rice [21], we base our analysis on the effective (pseudoatom) Hamiltonian for N ions and NZ sp-valence electrons. This Hamiltonian is derived by evaluating the electronic free energy of an inhomogeneous metal to second order in the electron-ion pseudopotential; it has the form

$$\mathcal{H}=\sum_{i=1}^{N}\frac{\mathbf{p}_i^2}{2m}+U_0[\rho_0(\mathbf{r}),n_{\mathrm{el}}(\mathbf{r})]+\sum_{i<j}V_{\mathrm{eff}}(\mathbf{R}_i,\mathbf{R}_j;n_{\mathrm{el}}(\mathbf{r})), \tag{1}$$

where $\mathbf{p}_i$ is the momentum of the ith atom with mass m, $V_{\mathrm{eff}}(\mathbf{R}_i,\mathbf{R}_j;n_{\mathrm{el}}(\mathbf{r}))$ is the effective pair potential between ions i and j located at $\mathbf{R}_i$ and $\mathbf{R}_j$, respectively, and $\rho_0(\mathbf{r})$ and $n_{\mathrm{el}}(\mathbf{r})$ are the corresponding reference jellium and electron densities. The functional U_0 is a structure independent contribution to the energy which is, however, dependent on the electron and jellium densities. In the following discussion, we use atomic units for length ($1a_0=0.529\,177$ Å) and energy (1 a.u.$=27.116$ eV).

Because of the importance we place on developing a qualitative understanding of the relationship between the structure of the liquid metal-vapor interface and the underlying atomic iterations, we now focus attention on how a useful approximate model of that interface can be developed.

A. Effective pair potential

The evaluation of the pair interaction portion of Eq. (1) requires knowledge of the electron response function for the inhomogeneous system, the calculation of which is itself a rather tedious task. The latter can be circumvented by invoking the local density approximation (LDA) in the calculation of the interionic potential functional [21,25,19]. This approximation is valid in the limit of slowly varying electron density, yet, we expect it to be at least qualitatively correct near a metal surface. The pair potential contribution is then expressed as

$$V_{\mathrm{eff}}(\mathbf{R}_i,\mathbf{R}_j;n_{\mathrm{el}})=V_H(|\mathbf{R}_i-\mathbf{R}_j|;\tfrac{1}{2}[n_{\mathrm{el}}(\mathbf{R}_i)+n_{\mathrm{el}}(\mathbf{R}_j)]), \tag{2}$$

with $V_H(R;n_{\mathrm{el}}^{\mathrm{LDA}})$ the interaction between two ions separated by $R=|\mathbf{R}_i-\mathbf{R}_j|$ in a homogeneous fluid with electron density $n_{\mathrm{el}}^{\mathrm{LDA}}$. V_H in turn is given by

$$V_H(R;n_{\mathrm{el}}^{\mathrm{LDA}})=\frac{Z^{*2}}{R}\left(1-\frac{2}{\pi}\int_0^{\infty}\frac{F_N(q)\sin(qR)}{q}dq\right)+W_{\mathrm{corr}}(R). \tag{3}$$

In Eq. (3), the first term is due to the direct Coulomb repulsion between ions with effective valence charge Z^*. For a nonlocal pseudopotential, the effective valence charge is related to the true valence charge Z and the depletion hole charge ρ_d, e.g., in the EIMP scheme Z^* is defined by $Z^{*2}=Z^2-\rho_d^2$ [36]. The depletion hole charge originates from the orthogonality condition between the valence and core electron wave functions. When a local model potential, like the modified empty-core model potential, is used instead, it is customary to set the effective charge Z^* equal to the true valence charge Z. The second term in Eq. (3) is an indirect interaction mediated by the conduction electrons, the so-called band structure energy; it tends to offset the effect of the strong Coulomb repulsion and thus lowers the energy of the system. The principal element of this contribution is the normalized energy-wave-number characteristic $F_N(q)$ which in the full theory is defined in terms of the matrix element of the bare pseudopotential along with the wave-number dependent nonlocal screening fields. We stress here that both $F_N(q)$ and ρ_d are functions of the electron density, though the explicit character of those density dependences is contingent upon the particular form of pseudopotential representation used. Several other terms are commonly incorporated in the expression for the effective pair interaction potential, and their cumulative contribution is denoted as $W_{\mathrm{corr}}(R)$ in Eq. (3). These other terms include the Born-Mayer core-core re-

pulsion potential [37] and the polarization (dispersion) potential which arises from the van der Waals attraction between the ion cores [20]. For liquid alkali metals, these contribution to the effective pair potential have been demonstrated to have negligibly small effect on the longitudinal density distribution in the liquid-vapor interface [19], but we find that not to be the case for liquid Hg when the local model potential formulation is used.

To calculate the effective pair interaction term, one must specify the pseudopotential and the local-field factor which corrects the random phase approximation dielectric function for the exchange and correlation effects among valence electrons [2]. We have chosen to work with the form of the local-field function proposed by Ichimaru and Utsumi [38]; this function satisfies the electron gas sum rules and its parametrized form is particularly suitable for use in computer simulations. Having stated these choices we remind the reader that the pseudopotential representation is not unique, so there is considerable freedom with respect to selection of the form of the pseudopotential for any given problem. Discussions of the advantages and disadvantages of different pseudopotential schemes can be found in the literature [2].

The theoretical description of the electronic structure of liquid Hg is complicated by the presence of a filled *d* band slightly below the conduction band, which suggests that *sd* coupling cannot be ignored. A generalized pseudopotential which includes valence-band–*d*-band interaction as well as *d*-orbital overlap has been developed by Moriarty [32,39]. Nevertheless, pursuing the goal of simplicity, we employ a local pseudopotential representation based on the Ashcroft [40] empty-core model potential with a simple additive correction. As will be shown below, this simplified potential supports a liquid mercury structure which agrees well with that obtained from available experimental data.

The bare empty-core model potential has the form

$$\omega_{\mathrm{bare}}(r)=\begin{cases}0 & \text{for } r<R_c\\ -\dfrac{Z}{r} & \text{for } r>R_c\,,\end{cases} \tag{4}$$

where R_c is the empty-core radius, a single parameter that characterizes the atomic properties. The form for the potential displayed in Eq. (4) has the practical advantage that the energy-wave-number characteristic $F(q)$ has the analytic form

$$F(q)=\frac{\Omega q^2}{8\pi}\left(\frac{1}{\epsilon(q)}-1\right)|\omega_{\mathrm{bare}}(q)|^2, \tag{5}$$

were Ω is the volume per atom ($\Omega=\rho^{-1}$), $\omega_{\mathrm{bare}}(q)$ is the Fourier transform of the bare pseudopotential, and $\epsilon(q)$ is the test-charge dielectric function which, in turn, is computed in terms of the random phase approximation (RPA) (Hartree) static dielectric function and the local-field factor [19]. The physical basis of the empty-core potential is derived from the ''cancellation theorem'' [1], which establishes that, to a first approximation, the true potential felt by a valence electron inside the core region, $r<R_c$, is effectively zero. R_c is typically adjusted to fit some experimental datum; the resulting value is usually found to be close to the accepted ionic radius. For heavy polyvalent metals, nonlocal effects, such as the relativistic contribution to the binding of the *s* electrons relative to that of the *p* electrons, become pronounced. Integrating such nonlocal effects into the empty-core model potential framework is known [1,41] to decrease the value of the empty-core radius R_c.

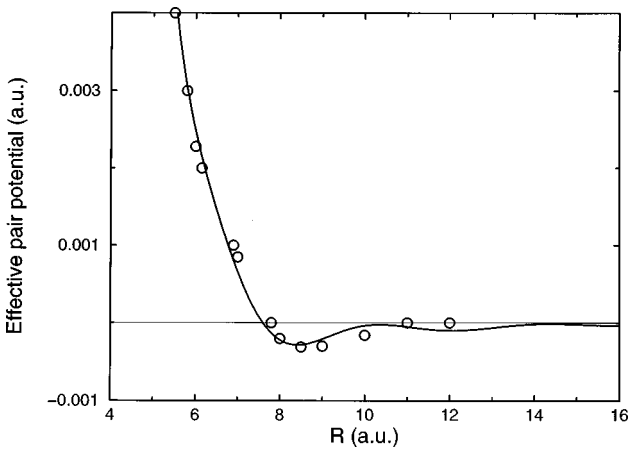

FIG. 1. Effective pair potential for liquid mercury at 20 °C (experimental density 0.0407 atom/Å^3). Solid curve: modified empty-core model potential. Circles: corrected optimized model potential (OMP) of D'Evelyn and Rice [20].

Since it is only a rough approximation to the ''true'' pseudopotential, the pair distribution function $g(R)$ and the static structure factor $S(q)$ of bulk liquid Hg calculated using the naive empty-core model of the pseudopotential deviate markedly from those obtained experimentally. The source for this discrepancy is the erroneous shape of the effective pair interaction potential [calculated via Eq. (3) with $W_{\mathrm{corr}}=0$] at typical bulk liquid densities; this potential has a minimum at a distance close to the nearest-neighbor spacing in a close-packed lattice. In contrast, the ''true'' effective pair potential calculated from an accurate relativistic core pseudopotential [32] is predominantly repulsive. D'Evelyn and Rice [20] have described how a crude pseudopotential treatment can be corrected via inclusion of physically meaningful additional terms. The resultant potential they constructed for Hg is more difficult to use in simulations than we think desirable for a simple model. We have found that addition of a single correction term, in the form of the Born-Mayer exchange repulsion, can improve the model potential sufficiently to make it useful for reliable predictions of the structure of the liquid. We write the Born-Mayer exchange repulsion in the form

$$V_{\mathrm{BM}}(R)=A_{\mathrm{BM}}\exp(-B_{\mathrm{BM}}R), \tag{6}$$

with A_{BM} and B_{BM} adjustable parameters. Then the total pair interaction energy is calculated via Eq. (3) by using Eq. (5) and setting $W_{\mathrm{corr}}(R)=V_{\mathrm{BM}}(R)$. As is illustrated in Fig. 1, the parameter values $R_c=0.915$ a.u., $A_{\mathrm{BM}}=200$ a.u., and $B_{\mathrm{BM}}=2.0$ a.u. generate an effective pair potential which is very much like the one constructed by D'Evelyn and Rice from a more sophisticated nonlocal treatment [20]. Our model pseudopotential also agrees well with the generalized pseudopotential (with filled *d* band) of Moriarty [42] and the pseudopotential derived by Jank and Hafner [32]. In Fig. 2 we display the density dependence of the effective pair in-

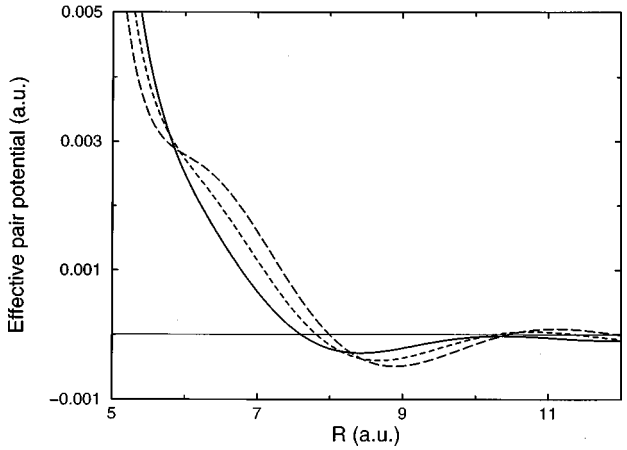

FIG. 2. Density dependence of the effective pair potential for liquid mercury. Solid curve: $\rho_{\text{bulk}}=0.0407$ atom/Å^3 (at 20 °C). Dashed curve: $\rho=0.8\rho_{\text{bulk}}=0.0326$ atom/Å^3. Long dashed curve: $\rho=0.7\rho_{\text{bulk}}=0.0285$ atom/Å^3.

teraction for liquid Hg. As shown in Fig. 3, the pair correlation function of bulk liquid Hg predicted using the effective interaction derived from our model pseudopotential is in good agreement with experimental data at 20 °C and 200 °C [31].

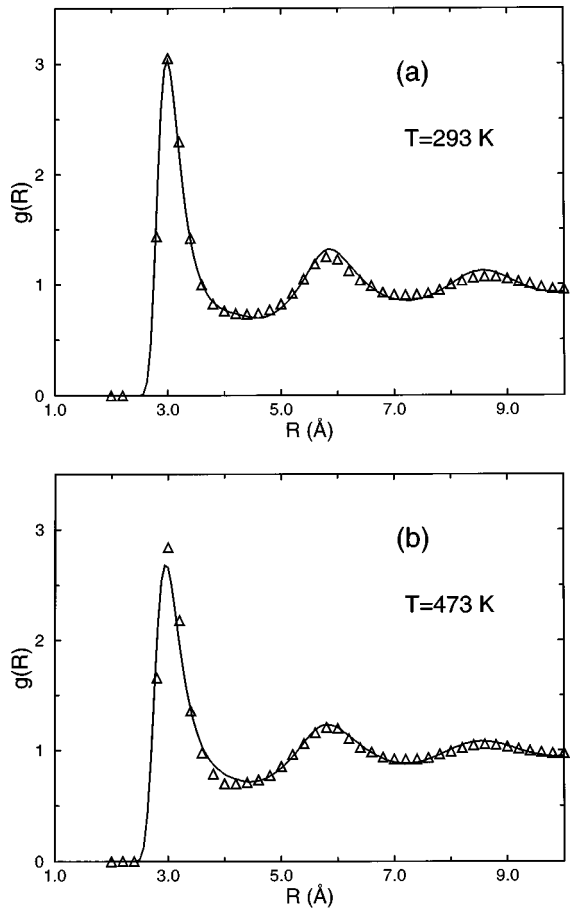

FIG. 3. Pair correlation function for bulk liquid mercury at 20 °C (a) and 200 °C (b). Solid line: results of the Monte Carlo simulations of the bulk liquid using the modified empty-core model potential. Triangles: experimental data of Bosio *et al.* [31].

Finally, it must be stressed that the model pseudopotential just described cannot account for the metal-to-nonmetal transition which occurs across the liquid-vapor interface, hence does not accurately represent the low density limit of the pair interaction functional.

In executing the simulations we cut off the effective pair potential at a distance $(19.9a_0)$ that is slightly less than half of the length of the simulation slab (which has dimensions $L_0\times L_0\times 2L_0$). Values of $V_H(R;n_{\text{el}}^{\text{LDA}})$, as functions of R and $n_{\text{el}}^{\text{LDA}}$, were tabulated and interpolated as described in our earlier work [19]. The density dependence of the pair interaction function at densities below about one-third of the bulk liquid Hg density was ignored. On average, only about 2–3 % of the atoms in the simulation slab are in the region where the average electron density is less than one-third of the bulk value. This condition on the low density behavior of the pair interaction function has far less effect on the structure than does the use of the local density approximation in the calculation of the structure independent energy and the pair potential.

B. Structure independent energy

In order to evaluate the potential part of the pseudoatom Hamiltonian given by Eq. (1), one needs to specify the functional form of a reference profile. Our simulations are carried out for a slab of ions with two free surfaces perpendicular to the z axis and using the jellium distribution

$$\rho(z,z_0,\beta)=\frac{\rho_{\text{bulk}}}{1+\exp[(|z|-z_0)/\beta]}, \tag{7}$$

where z_0 is the position of the Gibbs dividing surface and β measures the width of the inhomogeneous region of the profile. This distribution is normalized by setting $\rho_{\text{bulk}}=N/2Az_0$, where N is the total number of atoms in the slab and A is the area of one free face of the slab. The parameters z_0 and β are varied to obtain the best fit of Eq. (7) to the instantaneous ionic configuration [22,19].

Given the reference profile (7), and assuming that the electron density distributions in the x and y directions are uniform (because the ion density distributions in those directions are uniform), the electron density distribution in the z direction can be obtained by solving the one dimensional Kohn-Sham [3] equation

$$\left[-\frac{\hbar^2}{2m}\nabla_z^2+V_{\text{eff}}(z)\right]\psi_N(z)=\varepsilon_N\psi_N(z), \tag{8}$$

with $V_{\text{eff}}(z)$ an effective potential that includes the electron-positive background interaction and the exchange-correlation potential. Self-consistent solutions to the Kohn-Sham equation were obtained using the method proposed by Eguiluz *et al.* [30].

The structure independent energy U_0 can then be calculated for any given ionic configuration as a function of the corresponding electron density $n_{\text{el}}(\mathbf{r})$ and the reference (positive) charge density $\rho_0(\mathbf{r})$. It generally is defined via

$$U_0(\rho_0(\mathbf{r}),n_{\text{el}}(\mathbf{r}))=E_{\text{kin}}+E_{\text{es}}+E_{\text{xc}}+E_{\text{ps}}. \tag{9}$$

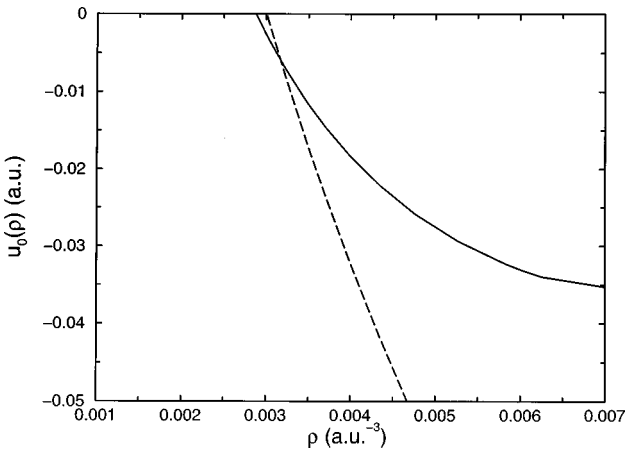

FIG. 4. Structure independent energy (no electrostatic term) per atom for liquid mercury: uncorrected (---), with empirical corrections (—). Bulk experimental density at 20 °C $\rho_{\text{bulk}}=6.03\times10^{-3}$ a.u.$^{-3}=0.0407$ atom/Å^3.

In Eq. (9), E_{kin} is the kinetic energy, which can be calculated from the solution of the relevant Kohn-Sham equation [30]; E_{es} is the electrostatic energy, which arises from the lack of coincidence of the electron and ion density distributions in the liquid-vapor interface; and the last two terms, E_{xc} and E_{ps}, are the exchange-correlation energy and the electron-ion pseudopotential interaction, respectively. In going from one pseudopotential representation to another, the term in Eq. (9) which changes is E_{ps}. For an inhomogeneous metal this term can be written as

$$E_{\text{ps}}=2A\int_0^\infty dz\,\rho_0(z)\epsilon_{\text{ps}}[n_{\text{el}}(z)], \tag{10}$$

where ϵ_{ps} assumes the following from in a local pseudopotential representation:

$$\epsilon_{\text{ps}}=3\int_0^1 f(\eta,\eta)\,\eta^2 d\eta-\left[\frac{2\pi Z}{\Omega}\lim_{q\to0}\frac{1-F_N(q)}{q^2}+\frac{Z^2}{\pi}\int_0^\infty F_N(q)dq\right]+\left(\frac{C_1}{r_s}+\frac{C_2}{r_s^2}\right). \tag{11}$$

In Eq. (11), $r_s=[(3/4\pi)n_{\text{el}}^{-1}]^{1/3}$ is the radius of a sphere which contains on average one electron and $\eta=k/k_F$. The first term in Eq. (11) is the first order correction to the system energy from the electron-ion pseudopotential, whereas the terms grouped inside the square brackets are, respectively, second order corrections. In order to compensate for the failure of the bare pseudopotential to ensure the mechanical stability of the model system, as well as to yield the correct value for the heat of vaporization at the experimental bulk density, it is necessary to introduce corrections to the structure independent energy [19,22]. These empirical corrections are embedded in the last contribution to ϵ_{ps} in Eq. (11), and their importance is demonstrated in Fig. 4.

TABLE I. Nonlocal ion pseudopotential parameters (in atomic units) for Hg. $r_{\max}$ is the maximum value of r in the radial wave function.

l	E_{1l}	R_l	B_{1l}	$\overline{B}_{1l}$	$r_{\max}$
0	0.689 078 6	1.8	1.180 163	0.700 763	35.0
1	0.454 565 0	1.7	1.119 794	0.426 535	45.0
2	0.210 882 2	3.0	0.669 270	0.638 592	55.0

III. SIMULATION TECHNIQUE

We have carried out self-consistent Monte Carlo simulations of liquid Hg at 20, 100, and 200 °C, using the Metropolis scheme [43]. All of the simulations were carried out on systems composed of 1000 ions in a slab geometry, with initial dimensions $L_0\times L_0\times 2L_0$, with periodic boundary conditions in the x and y directions, and with free surfaces in the $\pm z$ directions. The linear dimension of the simulation box, L_0, is defined such that the initial density of the slab matches exactly the known bulk atomic density ρ_{bulk} at the temperature of interest. The coordinate system is chosen so that the center of mass of the slab is positioned at the origin, $z=0$. Starting configurations for each run were generated in two steps. First, each particle was assigned a randomly chosen position within the slab boundaries. Second, the configurations containing core-core overlaps were eliminated by a force-based Monte Carlo simulation which uses a scaled Lennard-Jones potential for the ion core interaction.

In the course of a simulation ions are moved sequentially, one at a time, and the new configurations are accepted or rejected according to the standard procedure [43] by consulting the appropriate Boltzmann factors. The length of a run is conventionally measured in passes; each pass corresponds to 1000 test moves with one move per particle. In order to ensure that we sample only the equilibrium configurations of the ions, it is necessary to exclude several tens of thousands of passes from the initial stages of the simulation when collecting the final statistics.

To obtain the longitudinal ion density distribution, a histogram of particle positions relative to the position of the center of mass of the slab is compiled during the course of the simulation run. The density profiles from opposite halves of the slab are then averaged. The in-plane structure of the model system is described by the transverse pair correlation function, which we have calculated for thin sections parallel to the interface [19]. For a more detailed description of the numerical algorithms involved in the calculation of the interfacial structure we refer the interested reader to our previous publications.

IV. RESULTS

A. EIMP nonlocal pseudopotential

We consider first the results of simulations in which the EIMP nonlocal pseudopotential was used. This pseudopotential has the form [36]

$$V_{\text{ps}}^{\text{ion}}(r)=\sum_l\,[V_l^{\text{av}}(r)+\{V_{1l}(r)-V_l^{\text{av}}(r)\}]|l\rangle\langle l|, \tag{12}$$

where $V_l^{av}(r)$ is a pseudopotential average over all states other than the first valence state for a given angular momentum l. Details of the calculation of $V_l^{av}(r)$ and $V_{1l}(r)$ can be found in our earlier papers [25]. The parameters of the EIMP pseudopotential we used are displayed in Table I.

The simulations were carried out for 76 000 passes, with each pass consisting of 1000 configurations. We show in Fig. 5 a comparison of the calculated and experimental pair correlation functions for bulk liquid Hg at 20 °C, and in Fig. 6 a comparison of the calculated and experimental longitudinal density distributions in the liquid-vapor interface at the same temperature. We note that the positions of the peaks and troughs of the calculated and measured pair correlation functions are very nearly the same. Indeed, all the major features of the pair correlation function of liquid Hg, including the asymmetry in the shape of the first peak, are successfully reproduced. We also note that the agreement between the calculated and observed longitudinal density distributions is very good; both the locations and the amplitudes of the peaks in the longitudinal density distribution are well described by the calculations reported.

B. Model local pseudopotential

We now consider the results of simulations using the model local pseudopotential described in Sec. II. For each of the temperatures considered herein (20, 100, and 200 °C), Monte Carlo simulations using the slab configuration described in Sec. III were carried out for 36 000 passes. As was found to be the case in our previously reported study of the structures of the liquid-vapor interfaces of the alkali metals [19], these computations are much faster than those based on the use of the EIMP nonlocal pseudopotential. In particular, in real time each pass with the EIMP nonlocal pseudopotential is much longer than one with the model local pseudopotential and, as indicated, fewer passes are required before equilibrium is achieved.

A first test of our simulations is the demonstration that the bulk structure of liquid Hg is adequately reproduced. In Fig. 7 we compare the pair correlation function $g(R)$ calculated for the innermost stratum of the simulation slab (the one most remote from the interface) with that obtained from a simulation of uniform density liquid Hg in a cell defined by conventional cyclic boundary conditions in three dimensions. The agreement between the results of the two simulations at each of the temperatures sampled implies that the bulk region of the liquid is properly sampled using the geometry and boundary conditions defined in Sec. III.

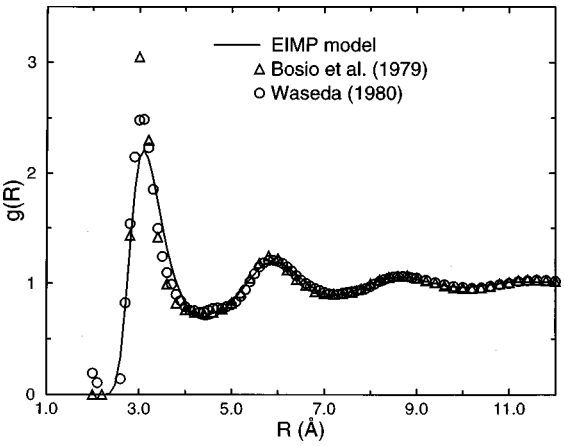

FIG. 5. Comparison of the pair correlation function for bulk liquid Hg calculated using the nonlocal EIMP pseudopotential and the experimental pair correlation function, at 20 °C. The experimental data of Bosio *et al.* [31] and those of Waseda [47] are shown.

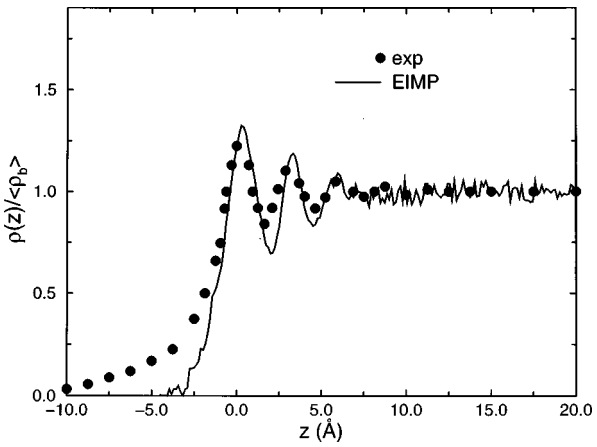

FIG. 6. Comparison of the longitudinal density distribution in the liquid-vapor interface of Hg calculated suing the nonlocal EIMP pseudopotential and the experimental longitudinal density distribution [7].

At 20 °C, the surface energy of liquid Hg obtained from our calculations is 536 ergs/cm^2, in very good agreement with the experimental value of 545 ergs/cm^2 [44]. It is known that not far from the melting point the experimental surface tension of liquid Hg varies linearly with temperature. Accordingly, the surface energy should be nearly independent of temperature for the range our simulations cover. However, our calculations yield a small increase in the surface energy when the temperature increases from 20 to 200 °C (about 6%). We attribute this discrepancy to residual inadequacies of the model local pseudopotential.

C. The longitudinal density distribution

The structural feature of most interest to us is the singlet ion density distribution across the liquid-vapor interface. This longitudinal density profile provides the most sensitive test of our calculations. Figure 8 displays a comparison of the longitudinal density profiles computed using the EIMP nonlocal pseudopotential, the model local pseudopotential, and that inferred from the x-ray reflectivity experiments of Pershan and co-workers [7]. Clearly, the results of the simulations using the model local pseudopotential correctly predict the existence and spacing of the strata in the liquid-vapor interface of Hg, but the widths of the strata are smaller and the amplitudes of the strata are larger than are characteristic of those in the longitudinal density distribution obtained experimentally. In both cases the stratification penetrates into the fluid interior for about three atomic diameters, and the interlayer spacing is on the scale of roughly one atomic diameter. The improved agreement with experiment obtained with the nonlocal pseudopotential is apparent; in that case the strata locations and widths are very much closer to the experimental values.

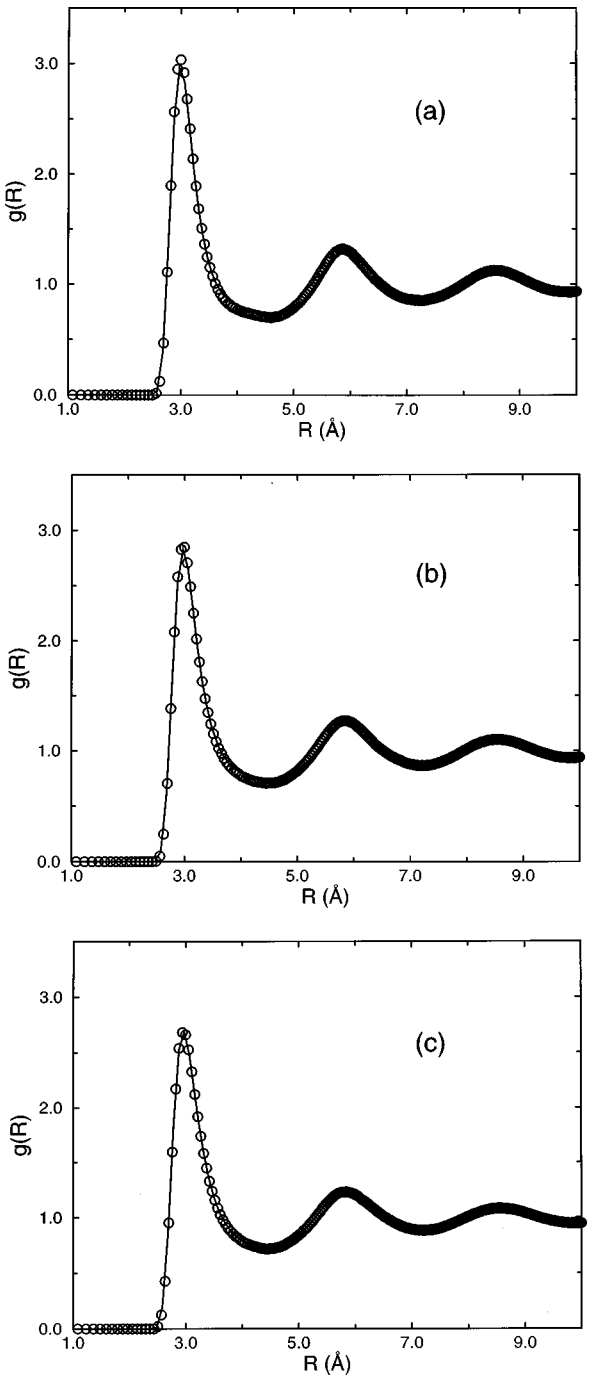

FIG. 7. Comparison of the transverse pair correlation function in the innermost stratum of the simulation box (solid curve) with that obtained in the a 3D bulk simulation (circle). (a) at 20 °C, (b) at 100 °C, (c) at 200 °C.

On the liquid side of the interface the oscillatory character of the longitudinal density distribution vanishes asymptotically as the distance into the bulk liquid increases, but at a smaller rate in the simulation data than in the experimental data. In fact, the amplitude of the density oscillations far from the interface found in the simulation results is consistent with the magnitude of the statistical noise observed in the transverse density distribution deep in the bulk liquid, as can be inferred from the data displayed in Fig. 9. And, as will be shown shortly, the difference between the amplitudes

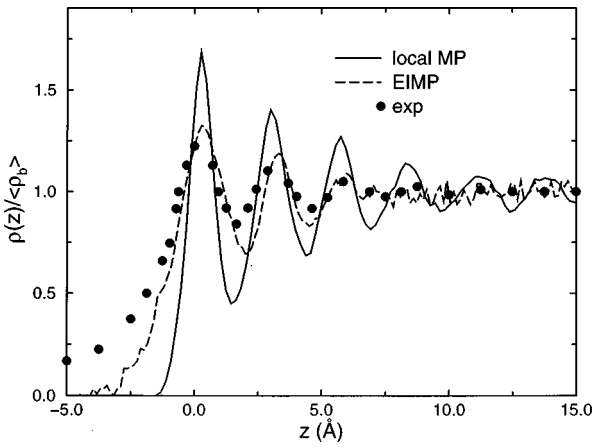

FIG. 8. Comparison of the longitudinal density distributions in the liquid-vapor interface of Hg calculated using the nonlocal EIMP pseudopotential (dashed line), the model local pseudopotential (solid line), and the experimental (room temperature) longitudinal density distribution (filled circles) [7].

of the first few peaks found in the simulation results and in the experimental results can be understood on the basis of capillary wave theory.

Both of the calculated longitudinal density distributions deviate most from that observed on the vapor side of the interface; the latter has a slowly decaying broad ''tail'' whereas the former do not. The inversion of the x-ray reflectivity data to yield the density on the vapor side of the liquid-vapor interface is subject to considerable experimental uncertainty. Indeed, it is possible that the ''tail'' in the longitudinal density distribution is due to the presence of a small amount of an alien material (e.g., HgO), which can have a profound effect on the surface properties [45]. We argue that the discrepancy between the observed and predicted longitudinal density distributions on the vapor side of the liquid-vapor interface of Hg is due to a combination of the limitations of the theoretical model and the inaccuracy of the experimental results.

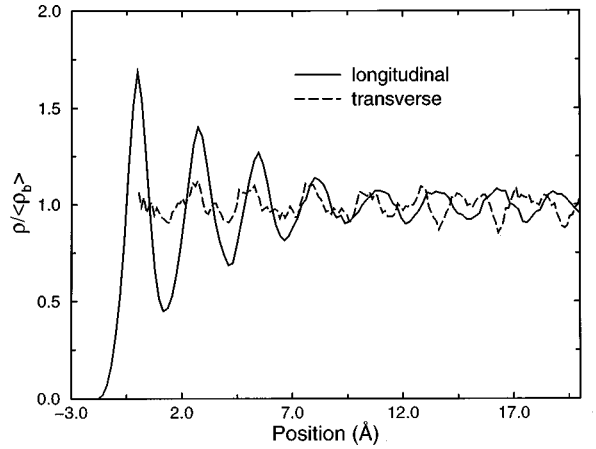

FIG. 9. Normalized transverse ion density distribution (long dashed curve), calculated for the innermost stratum of the simulation slab (model local pseudopotential) at 20 °C, superimposed on the corresponding longitudinal ion density profile (solid curve) from Fig. 8.

D. The transverse pair correlation function

We now examine the transverse (in-plane) pair correlation function in the liquid-vapor interface of Hg, which was calculated from histograms of the separations of all pairs of particles for each thin stratum sliced parallel to the interface. Thomas *et al.* have reported the results of a grazing incidence x-ray diffraction study of the liquid-vapor interface of Hg [13]. The major finding of this work was that the measured transverse structure function is very close to that of the bulk liquid Hg. Although this result agrees with the result obtained from a similar comparison of simulations of the pair correlation functions in the liquid-vapor interface and in the bulk of Cs, it must be recognized that the experimental x-ray diffraction signal is samples from all strata within the penetration depth of the incident x rays (about 30 Å). Thus the result of Thomas *et al.* eliminate the possibility that there is a highly ordered solidlike phase in the liquid-vapor interface of room temperature liquid Hg, but they cannot provide information about differences between the transverse structure of pairs of strata in the longitudinal density distribution. We display in Fig. 10 the transverse pair correlation functions calculated for the first two outer layers, corresponding to the regions which enclose first two high density peaks in the longitudinal density profile, together with $g(R)$ obtained from simulations of bulk liquid Hg at the same temperatures. The data in Fig. 10 show that for all layers beneath the outermost layer in the liquid-vapor interface the transverse pair correlation function of a layer is the same as the pair correlation function in the bulk liquid, just as in the previously reported studies of Cs [22,19], Ga [25], Al, In, and Tl [29]. The insensitivity of the transverse pair correlation function to the point local density implies that the in-plane structure is determined by some effective density which is defined by averaging the point density in a volume element that has linear dimensions comparable to an atomic diameter [22]. However, Fig. 10 also shows that for Hg the pair correlation function in the outermost layer of the liquid-vapor interface is different from that of the bulk liquid. The reduction of the peak amplitudes and the increase in peak separation are in the expected direction because the integrated density of the outermost peak is slightly less than that of the bulk liquid. On the other hand, the asymmetry of the first peak of $g(R)$ is very much more prominent than in the bulk liquid; at 20 °C it becomes a ''hump'' with considerable amplitude.

The exaggerated shoulder on the large R side of the first peak of the pair correlation function is of the type which some investigators believe is associated with dimerization. Our results do not support this interpretation. We have examined projections of the positions of the ion cores in the outermost layer of the liquid-vapor interface of Hg and can find no direct evidence for dimer formation.

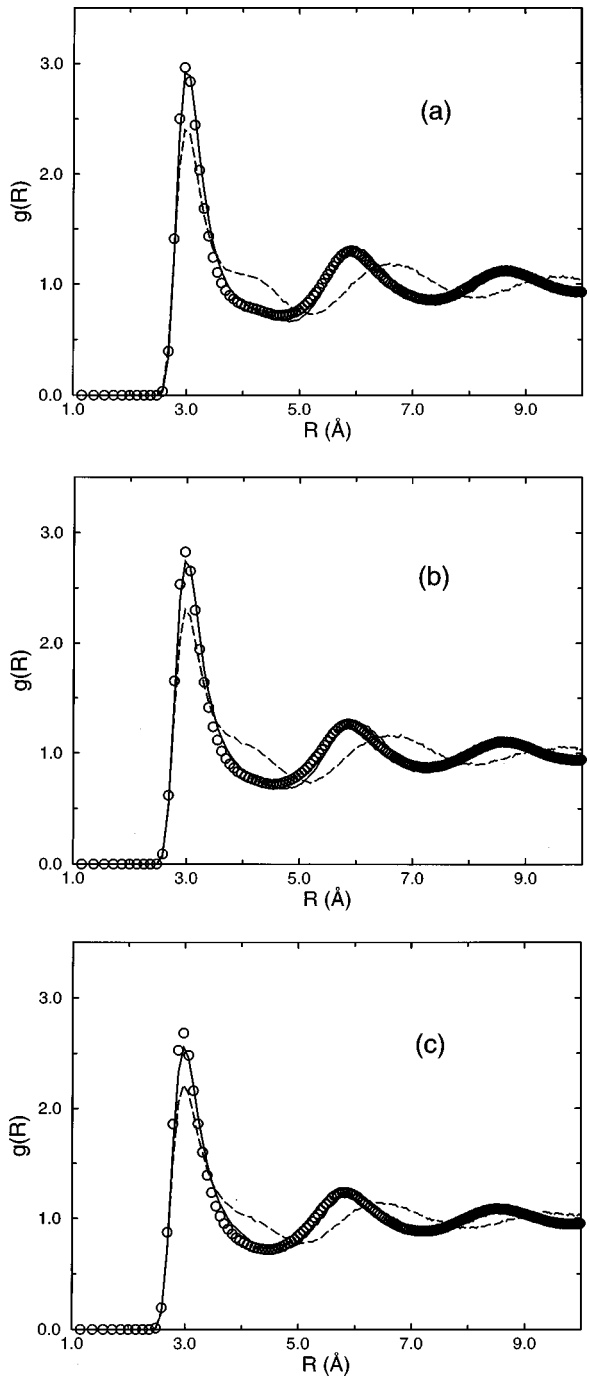

FIG. 10. Transverse pair correlation functions for selected layers from the liquid-vapor interface of Hg (model local pseudopotential). Bulk region (circle), second peak (solid curve), outermost peak (long dashed curve). (a) at 20 °C, (b) at 100 °C, (c) at 200 °C.

V. DISCUSSION

Although the longitudinal density profile in the liquid-vapor interface of Hg obtained using a model local pseudopotential is less accurate than that obtained using a nonlocal pseudopotential, all the important qualitative features of the experimental density profile are correctly predicted. This observation suggests that calculations based on the use of a model local pseudopotential can be used as a qualitative guide in the interpretation of experimental data. Moreover, if we can understand in simple terms the source of the discrepancy between the results of the simulations based on the different pseudopotentials, and develop a correction scheme, calculations based on model local pseudopotentials can be a practical guide to the understanding of a variety of phenomena and processes in complex inhomogeneous metals, e.g., alloys.

We first address the discrepancy between the longitudinal density profiles obtained from the simulations based on the model local pseudopotential and experiment. We begin our

analysis with a review of the process used to find the functional form of the density profile in the liquid-vapor interface which best fits the x-ray reflectivity data. Several models of the longitudinal density profile have been proposed [7,9], but we consider only the so-called distorted crystalline model (DCM) [7,9]. This model represents the liquid-vapor interface of a metal as a ''truncated solid,'' with successive layers in the interface separated from each other by the lattice spacing d. One function representing the properties of the DCM model is

$$\frac{\langle \rho(z) \rangle}{\rho_{\text{bulk}}} = \sum_{m=0}^{\infty} A_m \exp\left(\frac{-(z-md)^2}{2\sigma_m^2} \right). \tag{13}$$

In Eq. (13), the rms displacement of each layer is characterized by a Gaussian function, the width of which increases with penetration into the metal; in the limit $z \to \infty$ the uniform density of the bulk liquid metal is recovered. Note that the amplitude of the mth Gaussian term is

$$A_m = (1/\sqrt{2\pi})(d/\sigma_m).$$

The width σ_m^2, which measures the mean-square displacement of an atom from its lattice position, is commonly separated into two components: $\sigma_m^2 = \sigma_0^2 + m\overline{\sigma}^2$, where $\sigma_0^2 \equiv \sigma_0^2(T)$ alone is temperature dependent and $\overline{\sigma}^2$ is a constant. The value of $\overline{\sigma}$ is a measure of the increasing rms variation of the ''lattice'' position of a particle as the distance into the bulk liquid increases. The effect of temperature on the longitudinal density profile is accounted for by representing the long wavelength thermal excitations as capillary waves. Then

$$\sigma_0^2 = \sigma_{\text{int}}^2 + \frac{k_B T}{2\pi\gamma} \ln\left(\frac{q_{\max}}{q_{\min}} \right). \tag{14}$$

The first term on the right hand side of Eq. (14) is an intrinsic contribution to the width of a stratum in the longitudinal density profile [9], and the second term is the capillary wave theory representation of the mean-square fluctuations in the height-height correlation function [17]. The scale of the capillary wave amplitudes is set by $\gamma(T)$, the liquid-vapor interfacial tension at the given temperature. The largest wave factor ($q_{\max}$) contribution to the thermal excitation of the interface is defined (mod π) to be $2\pi/d$, whereas the smallest wave vector ($q_{\min}$) contribution depends on the size of the sample and is dictated by the resolution of the x-ray reflectivity data [7,9]. The interlayer spacing and the several contributions to the Gaussian width are model parameters that are varied to obtain the bet fit to the experimental data. As written, Eq. (13) represents a longitudinal density distribution that tends to zero rapidly on the vapor side of the interface. To account for the slowly decaying ''tail'' on the vapor side of the interface, Pershan and co-workers supplemented Eq. (13) with a series of Gaussian terms with center locations, amplitudes, and widths which are very different from those characterizing the rest of the longitudinal density distribution.

It is instructive to use the DCM to interpret both the experimental and the theoretical interfacial structure data. For this comparison we use the results of the simulations based on the model local pseudopotential. Magnussen *et al.* [7] reported that the following values of the DCM parameters provide the best fit to the intensity as a function of incident angle of the x-ray reflectivity from the liquid-vapor interface of Hg at room temperature: spacing between the first and the second layer, $d = 3.05 \pm 0.15$ Å, and between the subsequent inner layers $d = 2.76 \pm 0.20$ Å; $\overline{\sigma} = 0.50 \pm 0.05$ Å, $\sigma_0 = 0.95 \pm 0.05$ Å. Note the use of different spacings between the first and second layers and between all subsequent layer. The analogous fit to the model local pseudopotential simulation data at 20 °C with $d = 2.7 \pm 0.1$ Å, $\overline{\sigma} = 0.43 \pm 0.05$ Å, and $\sigma_0 = 0.64 \pm 0.02$ Å, is displayed in Fig. 11. Except for the use of a single interlayer spacing and the value of σ_0, the overall agreement between the values of the corresponding parameters is quite satisfactory. And, although the best fit of the simulation data uses the same interlayer spacing throughout the interface, the combined uncertainties of the values of the first interlayer spacing values for the experimental data ± 0.15 Å and the simulation data, ± 0.10 Å, is close to the difference in their values.

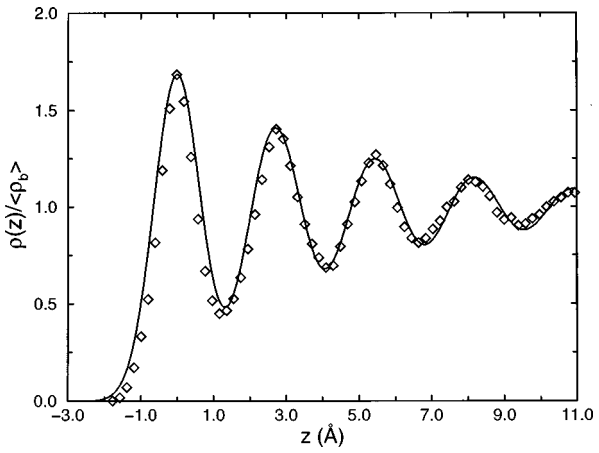

FIG. 11. Longitudinal ionic density profiles in the liquid-vapor interface of Hg at 20 °C: Monte Carlo simulation data (model local pseudopotential) (◇ ◇ ◇), the distorted crystalline model (—) with $d = 2.7$ Å, $\overline{\sigma} = 0.43$ Å, and $\sigma_0 = 0.64$ Å.

A similar comparison of the best fit of the nonlocal

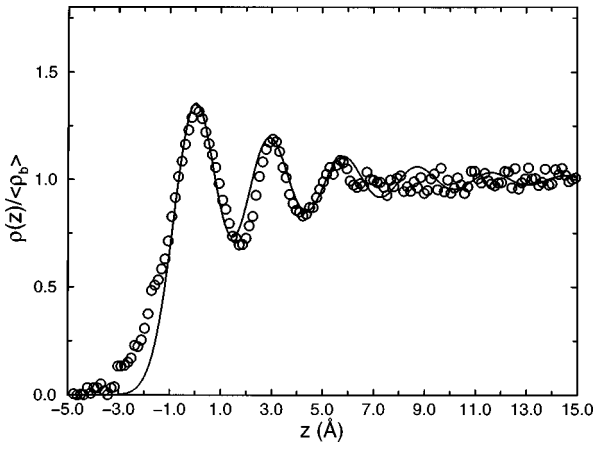

FIG. 12. Longitudinal ionic density profiles in the liquid-vapor interface of Hg at 20 °C: Monte Carlo simulation data (nonlocal EIMP pseudopotential) (○○○), the distorted crystalline model (—) with $d = 2.85$ Å, $\overline{\sigma} = 0.50$ Å, and $\sigma_0 = 0.85$ Å.

pseudopotential simulation data to the DCM (see Fig. 12) yields $d=2.85$ Å, $\sigma=0.50$ Å, and $\sigma_0=0.85$ Å. These values, aside from the use of a single interlayer spacing, are in good, but not perfect, agreement with those for the fit to the experimental data; again, it is the values of σ_0 that differ the most.

We note that the amplitudes of the oscillations of the longitudinal density profile, especially the height of the first peak, are strongly dependent on the value of σ_0. The difference in the peak heights between the experimental and theoretical longitudinal density distributions (Fig. 8) suggests that we examine the contributions to σ_0. We observe that the longest capillary wave that contributes to the thermal broadening of the observed longitudinal density distribution is much larger than can be supported by the simulation sample by the ratio of the macroscopic length corresponding to instrument resolution to the simulation slab length. Taking the shortest contributing capillary waves to be the same for both experiment and simulations, we estimate the magnitude of the logarithmic term in Eq. (14) for the experiment to be approximately three times bigger than it is for the simulation shape; this estimate is based on the reported values [7] for the pure capillary wave contribution to the rms displacement in the liquid-vapor interface of Hg, 0.8–1.0 Å, and the surface tension of Hg, $\gamma=485$ mN/m. Direct calculation of the capillary wave contribution to the broadening of the longitudinal density distribution obtained from the simulations requires knowledge of the surface tension of the model system, which can differ from the experimental surface tension, and which is not available from our calculations. For present purposes we substitute the experimental surface tension for that of the simulation model. Then we find that the magnitude of the mean-square displacement due to capillary wave excitations is 0.27 Å^2 ($\sigma_{\rm cap}^{\rm sim}=0.52$ Å). At 20 °C, from the known values of $(\sigma_0^{\rm sim})^2=0.41$ Å^2 and $(\sigma_{\rm cap}^{\rm sim})^2$, we find $\sigma_{\rm int}^2=0.14$ Å^2 ($\sigma_{\rm int}=0.37$ Å). Assuming that the experimental value of the intrinsic contribution is of comparable magnitude in the simulations and the real interface, a rough estimate of the experimental value of $\sigma_0^{\rm expt}$ can be obtained from $(\sigma_0^{\rm expt})^2 \approx \sigma_{\rm int}^2+3.0(\sigma_{\rm cap}^{\rm sim})^2$. The value thus deduced is 0.95 Å^2, leading to $\sigma_0^{expt}=0.97$ Å, which falls nicely within the error margins of the fit to the experimental data ($\sigma_0=0.95\pm0.05$ Å). This results implies that the height of the first peak in the simulated longitudinal density profile should be about 39% larger than that of the observed first peak, in very good agreement with the 35% increase in peak height we find. We conclude that the observed discrepancy between the amplitudes of the peaks in the simulated and experimental longitudinal density distributions is predominantly due to the difference in the magnitude of the contribution due to capillary wave excitation, which is governed by the difference between the sizes of the simulation sample and the experimental sample.

We now examine whether the temperature induced variation in the structure of the liquid-vapor interface of Hg can be rationalized with current theories. Figure 13 displays the normalized longitudinal density profiles of liquid Hg obtained from the quantum Monte Carlo simulations at 20, 100, and 200 °C, respectively. Just as in the case of Ga [8], the effect of increasing temperature on the interfacial structure of Hg is to decrease the amplitude of the surface oscillations;

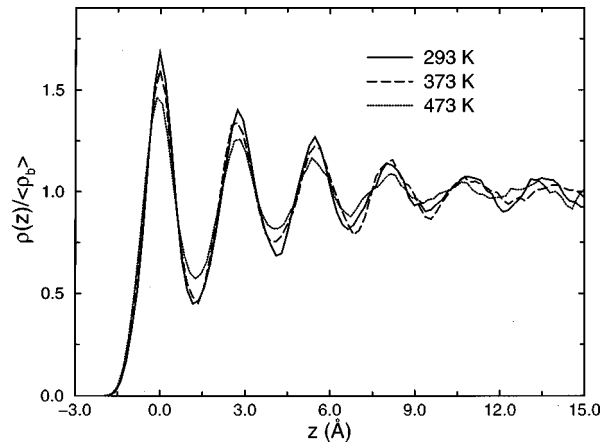

FIG. 13. Normalized longitudinal ion density profiles at 20 °C (solid curve), 100 °C (long dashed curve), and 200 °C (dotted curve). The simulation data (model local pseudopotential) are based on 36×10^6 configurations, from which the last 8×10^6 are used in collecting the final statistics.

the interlayer spacing is insensitive to temperature over the range studies. Arguments similar to those used to interpret the temperature dependence of the structure of the liquid-vapor interface of Ga also hold for Hg [25]. Nevertheless, we find it helpful to analyze the longitudinal structure of the liquid-vapor interface of Hg using the DCM described above. Despite slight deterioration in the quality of the fit at high temperature, all three data sets obtained from the Monte Carlo simulations are well described by the DCM. In particular, we find that the three temperature fits yield nearly identical values for d and $\overline{\sigma}$ (2.71 and 0.43 Å, respectively). Consequently, in the DCM the value of σ_0 dominates the temperature dependence of the longitudinal density profile. The values of σ_0 obtained from our simulation data are 0.64 Å at 20 °C, 0.68 Å at 100 °C and 0.74 Å at 200 °C. The assumption that the temperature dependence resides primarily in the capillary wave contribution leads to the inference that σ_0^2 varies linearly with T, because the surface tension of

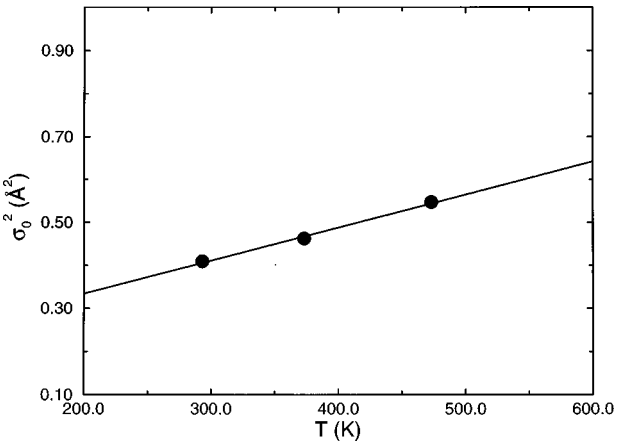

FIG. 14. Variation of the mean-square displacement $(\sigma_0)^2$ [see Eq. (14) in text] with temperature. Monte Carlo (MC) simulation data (filled circles), linear function (least squares) fit to the MC data (solid curve). The linear function intersects the vertical ($T=-273$ °C) at 0.17 Å^2 which is reasonably close to the value of $\sigma_{\rm int}^2$ (0.14 Å^2) used in text.

Hg varies linearly with T for the temperature range under consideration. As shown in Fig. 14, this expectation is fulfilled by the simulation data. A more detailed examination of the simulation data reveals that the temperature induced variation in the interface structure is almost entirely due to the capillary wave term, σ_{cap} in Eq. (14). A crude estimate of the surface tension of the simulation system can be inferred from the slope of the linear dependence of σ_0^2 on T (solid line in Fig. 14); the value obtained is about 20% larger than the experimental value of the surface tension at the melting point (498 mN/m).

Since the capillary wave theory treats $\gamma(T)$ as an input parameter, a calculation of this parameter from the simulation data is required to confirm the internal consistency of our interpretation of the structure of the liquid-vapor interface of Hg. An exact expression for $\gamma(T)$ in terms of the direct correlation function of the inhomogeneous fluid can be derived by considering the change in the grand potential associated with the increase of surface area induced by fluctuations in the position of the Gibbs dividing surface. Triezenberg and Zwanzig [46] have shown that

$$\gamma=\frac{kT}{4}\int_{-\infty}^{\infty}\frac{d\rho(z_1)}{dz_1}dz_1\int (x_2^2+y_2^2)\frac{d\rho(z_2)}{dz_2}c^{(2)}(\mathbf{r}_1,\mathbf{r}_2)d\mathbf{r}_2, \tag{15}$$

where $c^{(2)}(\mathbf{r}_1,\mathbf{r}_2)$ is the direct correlation function. In principle, if $g(r)$ [and, consequently, the total pair correlation function $h(r)=g(r)-1$] is available from, e.g., computer simulations, one can compute the direct correlation function using the Ornstein-Zernike relation,

$$g(r)-1=\frac{1}{(2\pi)^3}\int d\mathbf{q}\exp(-i\mathbf{q}\cdot\mathbf{r})\frac{\hat{c}^{(2)}(q)}{1-\rho\hat{c}^{(2)}(q)}. \tag{16}$$

Unfortunately, accurate calculation of $\gamma(T)$ by this route is not feasible for our simulations because the sample size is too small (the interfacial area is a square with edge length only eight atomic diameters).

It is an elementary consequence of thermodynamics that the temperature derivative of the surface tension determines the excess entropy associated with the interface; if $d\gamma/dT<0$ the excess entropy is positive. Although a positive excess entropy is usually associated with less order in the interface than in the bulk liquid, translating ''less order'' into a specific structure is not trivial, and it is not easy to determine the sign of the excess entropy associated with the structured interface that we have discussed in this paper. Recent experimental study, by Kolevzon and Pozdniakov, of the light scattered from thermally excited capillary waves in the liquid-vapor interface of Hg [45] demonstrate that $d\gamma/dT<0$. These investigators have proposed a thermodynamic analysis in which a liquid metal is considered to be a two-component fluid composed of positive ions and free delocalized electrons, respectively, each treated as an assembly of classical particles. They then show that $d\gamma/dT<0$ implies that the longitudinal electron density distribution must broaden as temperature increases. This inference is inapplicable to a real metal because of the assumption that the electron gas is classical. We show in Fig. 15 the normalized electron density profiles in the liquid-vapor interface of Hg at 20, 100, and 200 °C obtained from our self-consistent Monte Carlo simulations. As expected from the value of the Fermi temperature of the electron gas, our calculations show that the longitudinal electron density distribution is insensitive to temperature in the range considered.

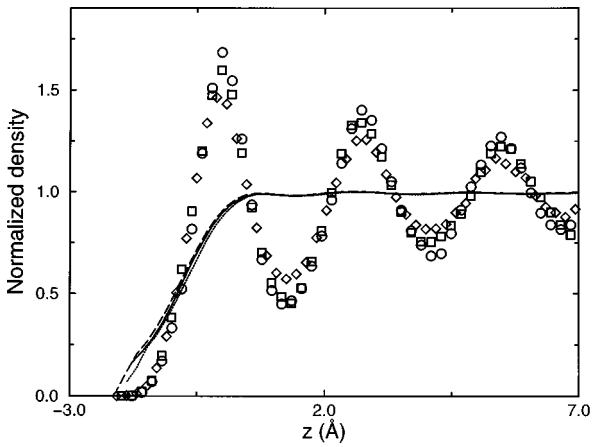

FIG. 15. Normalized longitudinal density profiles of liquid Hg: ion density distribution (circles) and electron density distribution (solid curve) at 20 °C, ion density distribution (squares) and electron density distribution (dotted curve) at 100 °C, ion density distribution (diamonds) and electron density distribution (long dashed curve) at 200 °C.

ACKNOWLEDGMENT

This work has been supported by a grant from the National Science Foundation.

[1] V. Heine and D. Wearie, in *Solid State Physics: Advances in Research and Applications*, edited by F. Seitz, H. Ehrenreich, and D. Turnbull (Academic, New York, 1970), Vol. 24; W. A. Harrison, *Pseudopotentials in the Theory of Metals* (Benjamin, New York, 1966).

[2] See, for example, J. Hafner, *From Hamiltonian to Phase Diagrams* (Springer-Verlag, Berlin, 1987); W. H. Young, Rep. Prog. Phys. **55**, 1769 (1992).

[3] P. Hohenberg and W. Kohn, Phys. Rev. **136**, B864 (1964); W. Kohn and L. J. Sham, *ibid.* **140**, A1133 (1965).

[4] *Computer Simulations in Chemical Physics*, Vol. 397 of *NATO Advanced Study Institue, Series B: Physics*, edited by M. P. Allen and D. J. Tildesley (Plenum, New York, 1993).

[5] P. Acioli, THEOCHEM **394**, 75 (1997).

[6] M. J. Regan, E. H. Kawamoto, S. Lee, P. S. Pershan, N. Maskil, M. Deutsch, O. M. Magnussen, and B. M. Ocko, Phys. Rev. Lett. **75**, 2498 (1995).

[7] O. M. Magnussen, B. M. Ocko, M. J. Regan, K. Penanen, P. S. Pershan, and M. Deutsch, Phys. Rev. Lett. **74**, 4444 (1995).

[8] M. J. Regan, P. S. Pershan, O M. Magnussen, B. M. Ocko, M. Deutsch, and L. E. Berman, Phys. Rev. B **54**, 9730 (1996).

[9] M. J. Regan, P. S. Pershan, O. M. Magnussen, B. M. Ocko, M.

Deutsch, and L. E. Berman, Phys. Rev. B **55**, 15 874 (1997).
[10] M. J. Regan, H. C. Tostmann, P. S. Perhan, O. M. Magnussen, E. DiMasi, B. M. Ocko, and M. Deutsch, Phys. Rev. B **55**, 10 786 (1997).
[11] N. Lei, Z. Huang, and S. A. Rice, J. Chem. Phys. **104**, 4802 (1996).
[12] N. Lei, Z. Huang, and S. A. Rice, J. Chem. Phys. **107**, 4051 (1997).
[13] B. N. Thomas, S. W. Barton, F. Novak, and S. A. Rice, J. Chem. Phys. **86**, 1036 (1987).
[14] E. B. Flom, Z. Cai, A. Acero, B. Lin, N. Maskil, L. Liu, and S. A. Rice, J. Chem. Phys. **96**, 4743 (1992).
[15] E. B. Flom, M. Li, A. Acero, N. Maskil, and S. A. Rice, Science **260**, 332 (1993).
[16] N. Lei, Z. Huang, S. A. Rice, and C. Grayce, J. Chem. Phys. **105**, 9615 (1996).
[17] J. S. Rowlinson and B. Widom, *Molecular Theory of Capillarity* (Clarendon, Oxford, 1982).
[18] See, for example, R. M. Townsend and S. A. Rice, J. Chem. Phys. **94**, 2207 (1991); D. K. Schwartz *et al.*, Phys. Rev. A **41**, 5687 (1990).
[19] D. Chekmarev, M. Zhao, and S. A. Rice, J. Chem. Phys. **109**, 768 (1998).
[20] M. P. D'Evelyn and S. A. Rice, J. Chem. Phys. **78**, 5081 (1983).
[21] M. P. D'Evelyn and S. A. Rice, J. Chem. Phys. **78**, 5225 (1983).
[22] J. G. Harris, J. Gryko, and S. A. Rice, J. Chem. Phys. **87**, 3069 (1987).
[23] J. G. Harris, J. Gryko, and S. A. Rice, J. Stat. Phys. **48**, 1109 (1987).
[24] A. Gomez and S. A. Rice, J. Chem. Phys. **101**, 8094 (1994).
[25] M. Zhao, D. Chekmarev, Z. Cai, and S. A. Rice, Phys. Rev. E **56**, 7033 (1997).
[26] M. Zhao, D. Chekmarev, and S. A. Rice, J. Chem. Phys. **108**, 5055 (1998).
[27] S. A. Rice, M. Zhao, and D. Chekmarev, in *Microscopic Simulation of Interfacial Phenomena in Solids and Liquids*, edited by S. R. Phillpot. P. D. Bristowe, D. G. Stroud, and J. R. Smith (Materials Research Society, Pittsburgh, 1998), Vol. 492, pp. 3–14.
[28] S. A. Rice and M. Zhao, Phys. Rev. B **57**, 13 501 (1998).
[29] M. Zhao, D. Chekmarev, and S. A. Rice, J. Chem. Phys. **109**, 1959 (1998).
[30] A. G. Eguiliuz, D. A. Campbell, A. A. Maradudin, and R. F. Wallis, Phys. Rev. B **30**, 5449 (1984).
[31] L. Bosio, R. Cortes, and C. Segaud, J. Chem. Phys. **71**, 3595 (1979).
[32] W. Jank and J. Hafner, Phys. Rev. B **42**, 6926 (1990).
[33] J. Hafner and W. Jank, Phys. Rev. B **42**, 11 530 (1990).
[34] V. Petkov and G. Yunchov, J. Non-Cryst. Solids **192-193**, 636 (1995).
[35] L. Ottaviano, A. Filipponi, A. DiCicco, S. Santucci, and P. Picozzi, J. Non-Cryst. Solids **156-158**, 112 (1993).
[36] C. H. Woo, S. Wang, and M. Matsuura, J. Phys. F **5**, 1836 (1975).
[37] T. L. Gilbert, J. Chem. Phys. **49**, 2640 (1968).
[38] S. Ichimaru and K. Utsumi, Phys. Rev. B **24**, 7385 (1981).
[39] J. A. Moriarty, Phys. Rev. B **5**, 2066 (1972); **5**, 16 (1977); **5**, 19 (1979).
[40] N. W. Ashcroft, Phys. Lett. **23**, 48 (1966).
[41] W. Jank and J. Hafner, Phys. Rev. B **41**, 1497 (1990).
[42] J. A. Moriarty, Phys. Lett. A **131**, 41 (1988).
[43] N. Metropolis, A. W. Rosenbluth, M. N. Rosenbluth, A. M. Teller, and E. Teller, J. Chem. Phys. **21**, 1087 (1953).
[44] B. C. Lu and S. A. Rice, J. Chem. Phys. **68**, 5558 (1978).
[45] V. Kolevzon and G. Pozdniakov, J. Phys.: Condens. Matter **9**, 6815 (1997).
[46] D. G. Triezenberg and R. Zwanzig, Phys. Rev. Lett. **28**, 1183 (1972).
[47] Y. Waseda, *The Structure of Non-Crystalline Materials — Liquids and Amorphous Solids* (McGraw-Hill, New York, 1980).